Journal of Materials Science: Materials in Electronics (2019) 30:746–752
https://doi.org/10.1007/s10854-018-0343-z

Butanol-assisted solvent annealing of $CH_3NH_3PbI_3$ film for high-efficient perovskite solar cells

Junpeng Mou[1,2,3] · Jian Song[1,2,3] · Min Che[1,2,3] · Yan Liu[1,2,3] · Yongshan Qin[1,2,3] · Heming Liu[1,2,3] · Lei Zhu[1,2,3] · Yulong Zhao[1,2,3] · Yinghuai Qiang[1,2,3]

Received: 4 July 2018 / Accepted: 8 November 2018 / Published online: 11 November 2018
© Springer Science+Business Media, LLC, part of Springer Nature 2018

Abstract

Due to the characteristics of low cost, simple process and high conversion efficiency, perovskite solar cells have become a research hotspot in recent years. In the structure of perovskite solar cell, perovskite active film plays an important role in sunlight absorption and electron–hole pair generation. This work focused on improving the quality of perovskite film by solvent annealing of perovskite film prepared with two-step spin-coating method. We chose n-butanol, a solvent with high boiling point, as an additive in CH_3NH_3I/isopropanol solution to execute the solvent annealing process. UV–Vis absorption spectra exhibited an enhancement in the absorbance of perovskite films with solvent annealing process. X-ray diffraction and scanning electron microscope measurements indicated that perovskite film had larger grain size after solvent annealing, especially when n-butanol content reached to 2% in the mixed solvents. The photovoltaic performance of perovskite solar cell was improved from 13.50% to the optimized 14.81%. This solvent annealing process could restrain the fast evaporation of solvent in CH_3NH_3I solution which is beneficial for perovskite film growth. It is found that this method has certain significance for the quality improvement of the perovskite film.

1 Introduction

Owing to the energy crisis and the environmental pollution, more and more attention has been focused on new energy materials and devices. As the renewable and massive properties of solar energy, solar cells are widely developed [1]. Silicon based solar cells is usually limited by the high cost and large energy consumption. Some novel solar cells, such as dye-sensitized solar cells or polymer solar cells, have the advantage in cost, but are suppressed by their lower power conversion efficiency and poor stability [2–6]. Organic–inorganic hybrid lead halide based perovskite solar cell, emerging in 2009, are promising photovoltaic device with the feature of low cost and high efficiency. The satisfying photovoltaic performance of perovskite solar cells originates from the excellent optical and electrical properties of perovskite materials, such as suitable bandgap, excellent light harvesting properties, long charge carrier lifetime, long electron–hole diffusion length, and the low crystallization temperature [7, 8].

Perovskite films, the core of perovskite solar cells, absorb the incident light and produce electron–hole pairs after being excited. Many researches have been implemented to improve the performance of perovskite layers in perovskite solar cells [9–16]. Khatiwada fabricated perovskite film by annealing perovskite precursor solution at 150 °C using one-step deposition method to achieve a high photovoltaic performance [17]. Wu improved the efficiency of PSCs to 13.5% by sequential two-step deposition with the absence of mesoporous scaffolds [18].

Electronic supplementary material The online version of this article (https://doi.org/10.1007/s10854-018-0343-z) contains supplementary material, which is available to authorized users.

✉ Jian Song
jsoong@cumt.edu.cn

✉ Yinghuai Qiang
yhqiang@cumt.edu.cn

[1] School of Materials Science and Engineering, China University of Mining and Technology, Xuzhou 221116, China

[2] The Jiangsu Province Engineering Laboratory of High Efficient Energy Storage Technology and Equipments, China University of Mining and Technology, Xuzhou 221116, China

[3] The Xuzhou City Key Laboratory of High Efficient Energy Storage Technology and Equipments, China University of Mining and Technology, Xuzhou 221116, China

Compared to one-step deposition method, the two-step deposition process could achieve a dense, smooth perovskite layer with superior crystallinity and good repeatability. To prepare high quality perovskite film in two-step deposition method, adding $TBAI_3$, CH_3NH_3I (MAI) or 4-tert-butylpyridine (TBP) in PbI_2 precursor could assist the forming of smooth and high quality films in the specific environment [19–21]. Additionally, solvent annealing was also reported to be an effective method to increase the perovskite grain size and crystallinity [22].

In this study, we explored a novel solvent annealing process for perovskite film in two-step deposition method. We introduced n-butanol in the solution of CH_3NH_3I/isopropanol (MAI/IPA). The addition of n-butanol is helpful to assist the crystal growth of perovskite film. We found that the photovoltaic performance of PSC achieved to 14.81% from 13.50% when the addition of n-butanol is 2% in MAI/IPA solution.

2 Experimental section

2.1 Fabrication of perovskite solar cells

F-doped SnO_2 (15 Ω/square, Nippon Sheet Glass) glass substrates were cut into 1.9 cm × 1.9 cm specification of the square. The edge of FTO glass was etched by 0.1 cm × 1.9 cm area with the laser etching machine. Then, the FTO glass were washed in ultrasonic processor for 30 min with optical glass cleaner, deionized water, ethyl alcohol (95%), isopropyl alcohol and ethyl alcohol (99%), successively. TiO_2 compact layer was prepared as early reports [23, 24]. The precursor solution was sprayed on the clean FTO glass at 450 °C. The spray solutions were prepared by diluting titanium diisopropoxide bis(acetylacetonate) with isopropanol in the ratio of 1:100 by volume. Subsequently, the TiO_2 paste (18NRT, Dyesol), diluted in alcohol in a mass ratio of 1:5.5, was spin-coated on the TiO_2 compact layer at 5000 rpm for 30 s, and then annealed at 500 °C for 15 min in a furnace under ambient air. The perovskite layer was fabricated by two step spin-coating method. The specific method would be described in "Solvent annealing process of the perovskite film" section in detail. After cooling to room temperature, 50 µL hole transport material (HTM) solution was spin-coated on the perovskite layer at 3000 rpm for 30 s. The HTM solution was prepared by dissolving 72.3 mg (2,2′,7,7′-tetrakis(*N,N*-di-*p*-methoxyphenylamine)-9,9-spirobifluorene) (spiro-OMeTAD), 28.8 µL 4-TBP, 17.5 µL of bis(trifluoromethylsulphonyl)imide (LiTFSI) in acetonitrile (520 mg/mL) in 1 mL chlorobenzene. Finally, the 70 nm of Ag as counter electrode was evaporated using thermal evaporator on the HTM-coated film.

2.2 Solvent annealing process of the perovskite film

The perovskite layer was deposited by two step spin-coating method. The methylammonium iodide (CH_3NH_3I, MAI) was dissolved in isopropanol, with a CH_3NH_3I/IPA solution of concentration of 15 mg/mL. For solvent annealing process, we added n-butanol in the MAI/IPA solution in the ratio of 1%, 2%, and 4% by volume. 1.3 mol/L PbI_2 (DMSO) solution in *N,N*-dimethylformamide was prepared at 70 °C, which was dripped onto the mesoporous TiO_2 film after infiltration and then spin-coated at 3000 rpm for 30 s. Subsequently, the CH_3NH_3I solution was spin coated on the PbI_2 (DMSO) film at 5000 rpm for 30 s and then annealed at 150 °C for 20 min in glove box.

2.3 Characterization

The microstructure and morphology of perovskite films were measured by X-ray diffraction (XRD, D8 ADVANCE, Bruker), scanning electron microscopy (SEM, SU8220, Hitachi). The photo-absorption properties of perovskite films were characterized by UV–Vis spectrophotometer (CARY 300 Conc). Time-resolved photoluminescence (TRPL) spectra of glass/perovskite film apparatus were measured by a time-resolved single-photon counting technology (Edinburgh FLS 980). The wavelength of exciting light was 200 nm. Photocurrent–voltage (J–V) characteristic curves of PSCs were recorded by an electrochemical workstation (Keithley, 2420 Source Meter). The cell was illuminated by a solar simulator (Oriel Sol 3A, Newport) under 100 mW/cm^2 irradiation, calibrated by a standard silicon solar cell (Oriel Instrument). A non-reflective metal aperture of 0.1 cm^2 was used to define the active area of the device and avoid light scattering through the sides. We applied reverse and forward scan between 1.0 and 0 V with the delay time of 40 ms. The incident photon-to-current conversion efficiency (IPCE) was measured using a power source (Newport 300W Xenon lamp, 66902) with a monochromator (Newport Cornerstone 260) and a power meter (Newport 2936-C).

3 Results and discussion

The addition of n-butanol in MAI/IPA solution has prominent influence on the microstructure of perovskite film. Figure 1 shows the XRD patterns of perovskite films using n-butanol in the volume ratio of 0%, 1%, 2%, and 4% to isopropanol. As shown in Fig. 1a, all the four patterns of perovskite films have strong diffraction peak located at 14.0°, 28.3°, and 31.7°. The three diffraction peaks correspond well

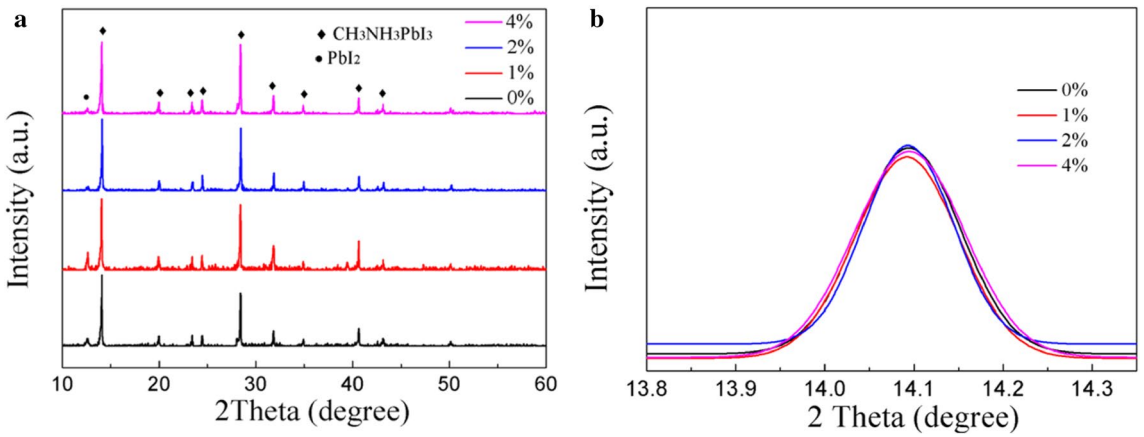

Fig. 1 **a** XRD patterns of perovskite films using n-butanol in the volume ratio of 0%, 1%, 2%, and 4% to isopropanol. **b** Enlarged patterns of perovskite films at the angle about 14.0

to the (110), (220), and (312) crystal planes of $CH_3NH_3PbI_3$. Additionally, the tiny diffraction peak at 12.7° belongs to PbI_2, indicating that all the perovskite films have PbI_2 impurities although most of PbI_2 has converted into the tetragonal $CH_3NH_3PbI_3$. This phenomenon usually appears in the fabrication process of $MAPbI_3$ via the two-step deposition because of the uncompleted conversion or perovskite decomposition [25, 26]. Figure 1b, enlarged patterns at the angle about 14.0, shows that the diffraction peak of perovskite films have varied half peak width. It is calculated by Scherrer's equation that the $CH_3NH_3PbI_3$ with n-butanol ratios of 0%, 1%, 2%, 4% has a grain size of about 53 nm, 59 nm, 67 nm, 54 nm. It could be concluded that perovskite film has larger crystal size after the n-butanol was introduced into the MAI/IPA solution. Additionally, the perovskite films fabricated using n-butanol, 1-pentanol, and propanetriol also present good crystallinity, as shown in Fig. S1. Moreover, the solvents are beneficial to restrain the appearance of PbI_2 impurity.

Figure 2 shows SEM images of $CH_3NH_3PbI_3$ active layers fabricated with different amount of n-butanol additive. The perovskite films prepared in this work are dense and uniform with almost full surface coverage, as shown in Fig. 2a–h. In Fig. 2e, f, we could find that the perovskite films are made of high-crystallinity grains with a size of 100–500 nm, and the sizes are varied as different amount of n-butanol are added in MAI/IPA solution. From the statistical results of perovskite grain size, we find that the introduction of n-butanol in the solution could improve the most probable grain size of perovskite films, and the largest size is obtained as the ratio of n-butanol is 2%. As we known, the boiling point of n-butanol is higher than that of isopropanol. In the formation process of perovskite films, the evaporation rate of solvents closely related with the perovskite grain size. The slow evaporation of solvent is beneficial to large perovskite grain growth. We think that is the reason for the larger perovskite grain after introducing n-butanol in MAI/IPA solution. As the small amount of n-butanol in MAI/IPA solution, the perovskite

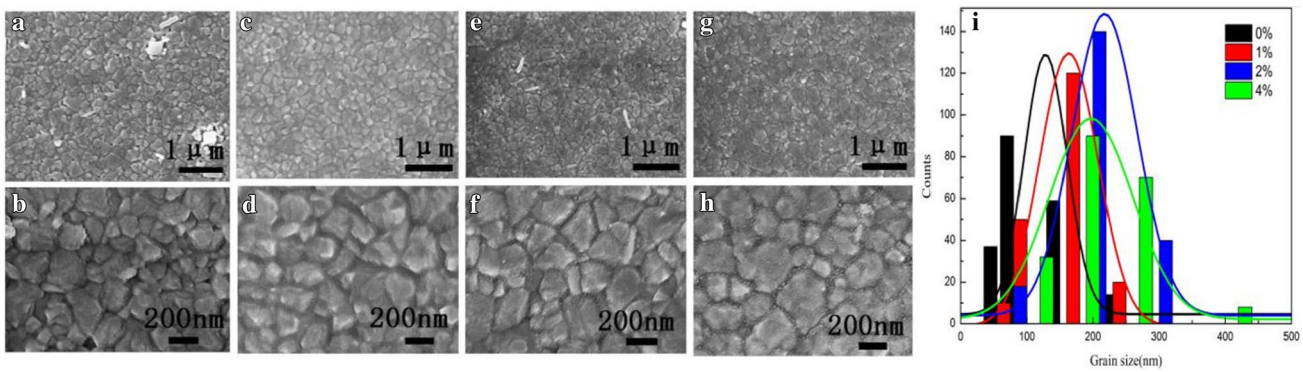

Fig. 2 SEM images for $CH_3NH_3PbI_3$ perovskite films fabricated by adding **a, b** 0%, **c, d** 1%, **e, f** 2%, **g, h** 4% n-butanol in MAI/IPA solution. **i** A histogram comparing the difference of perovskite grain size prepared by different amount of n-butanol additive based on 200 grains

film thicknesses do not change seriously, as shown in Fig. S2. We could clearly find that the stack architectures are composed of glass/FTO/compact TiO_2/mesoporous TiO_2/perovskite layer, and the film thicknesses vary from 342 to 357 nm. As for perovskite films prepared by n-butanol, 1-pentanol, and propanetriol solvents, the thicknesses change from 331 to 370 nm. The result reveals that organic solvents play import role in the growth of perovskite film because of their different volatility and viscosity.

The UV–Vis absorption spectra were applied to investigate the influence of n-butanol additive on the light absorption of corresponding perovskites films. As shown in Fig. 3, all the perovskite films perform strong absorption ability over the whole UV–Vis range. As the introduction of n-butanol in MAI/IPA solution, the deposited perovskite film present higher absorption performance as the larger perovskite grain sizes according to SEM results. The highest light absorption could be obtained when the ratio of n-butanol reached to 2%. As we known, high light absorption performance of active layer is the prerequisite condition for the high photovoltaic performance of solar cells [27]. Therefore, the proper addition of n-butanol in the perovskite film formation process is beneficial to get high performance perovskite solar cells. To further demonstrate the electrical and optical quality of perovskite films, we employed the TRPL spectra of glass/perovskite to detect the internal recombination in the perovskite layers. As we known, the recombination of electrons and holes is slow as the perovskite film has perfect crystallization and few defects [28, 29]. Therefore, in TRPL spectra, the recombination time is positively correlated with the quality of perovskite film. As shown in Fig. 3b, the perovskite films fabricated without or with n-butanol in MAI/IPA solution exhibited a life-time of 15.82 ns, 24.12 ns (1%), 46.84 ns (2%), and 15.78 ns (4%). This result demonstrates that n-butanol additive could assist to form a high quality perovskite film.

The J–V curves of the best-performing perovskite solar cells fabricated by different amount of n-butanol additive is shown in Fig. 4, and the corresponding photovoltaic performance parameters are summarized in Table 1. The pristine perovskite solar cell exhibits a conversion efficiency of 13.50%, with Voc of 0.96 V, Jsc of 19.51 mA/cm^2, and fill factor of 0.72. After the introduction of n-butanol, all the four parameters of perovskite solar cells increase. This result is agreed with SEM and UV–Vis measurements, as larger grain sizes and higher absorption could be obtained for perovskite film fabricated by n-butanol additive. The photovoltaic performance achieves to the highest when n-butanol ratio is 2% in MAI/IPA solution. In this condition, the perovskite film has the largest grain size which is good for accelerating charge transfer and decreasing charge recombination. Meanwhile, the perovskite film also presents the highest absorption ability which is beneficial to produce more excitons under illumination. The IPCE spectra and integrated Jsc are shown in Fig. 4b. The onset of photocurrent at 800 nm was consistent with the band gap of $CH_3NH_3PbI_3$ (~ 1.5 eV). The PSCs fabricated by n-butanol additive present higher quantum yield between 350 and 750 nm, compared to the pristine one. The integrated Jsc are very close to the tested short-current density from J–V. J–V hysteresis under different scan direction is a common phenomenon in perovskite solar cell which may prevent the correct evaluation of their photovoltaic performance [30]. Figure 4c shows the J–V curves of PSCs under reverse and forward scan based on 2% n-butanol additive. According to the specific photovoltaic parameters recorded in Table 1, the scan directions have evident influence on PSC. The PCE under forward scan is 81% of the reverse scan when 2% n-butanol is added while the value is 78% for the control device. The hysteresis index, an important indicator to evaluate the I–V curve hysteresis [31, 32], demonstrate that n-butanol is beneficial for decreasing the I–V hysteresis

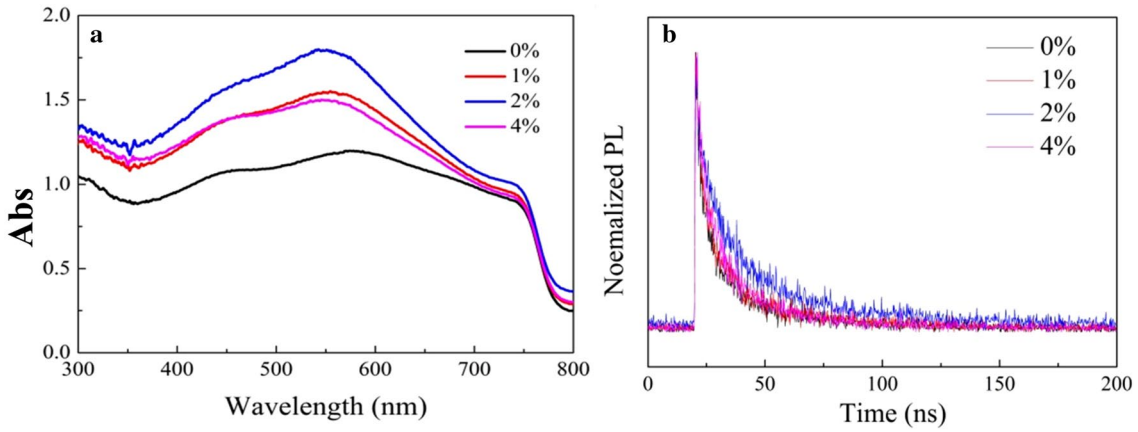

Fig. 3 **a** UV–Vis spectra and **b** TRPL spectra of perovskite films fabricated by different amount of n-butanol additive in MAI/IPA solution

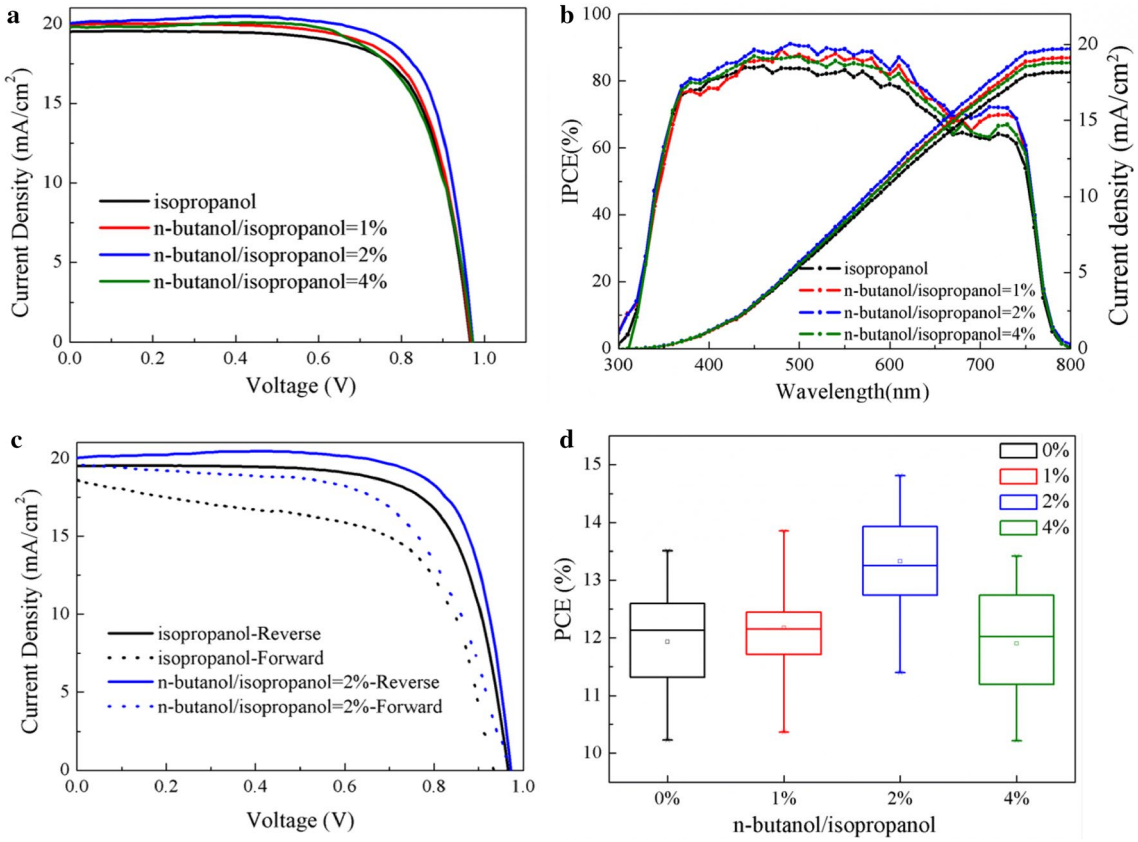

Fig. 4 **a** J–V curves of perovskite solar cells based on different amount of n-butanol additive in MAI/IPA solution, **b** IPCE spectra of PSCs, **c** the J–V curve of PSC fabricated by pure IPA and 2% n-butanol additive under reverse and forward scan direction, **d** statistical values of PCE of perovskite solar cells based on 30 independent devices

Table 1 Photovoltaic parameters of perovskite solar cells based on different amount of n-butanol additive in MAI/IPA solution

Solvents (n-butanol/isopropanol) (%)	Scan direction	J_{sc} (mA/cm^2)	V_{oc} (V)	FF	PCE (%)	Hysteresis index
0	Reverse	19.51	0.96	0.72	13.50	0.23
	Forward	18.60	0.94	0.61	10.59	
1	Reverse	19.98	0.96	0.72	13.85	–
2	Reverse	20.07	0.97	0.76	14.81	0.22
	Forward	19.75	0.97	0.62	11.81	
4	Reverse	19.79	0.97	0.70	13.42	–

effect of PSCs. The statistical photovoltaic performances of PSC devices based on different amount of n-butanol additive are shown in Fig. 4d. The average PCE increase dramatically from 12.12 to 13.40% after the n-butanol additive reached to 2%.

Figure 5 shows device stability in dry air without encapsulation for the perovskite solar cells fabricated with or without 2% n-butanol additive. It could be observed that the efficiency of the control perovskite solar cell decreases by 92% after 10 days, while the value is 71% for the device using n-butanol assisted perovskite film. The minor improvement of the stability is attributed to the larger grain size and less grain boundary of n-butanol assisted perovskite film.

As discussed above, we could find that n-butanol is an adequate candidate as an additive in perovskite precursor solution. This solvent has relatively low volatility because of its high boiling point, compared to isopropanol. In the solvent annealing process, the slowly evaporation of solvents is helpful for grain growth. However, as the isopropanol solvent of MAI solution is totally replaced by n-butanol, the corresponding PSC do not show higher photovoltaic performance as expected, as shown in Fig. 6. Additionally, we

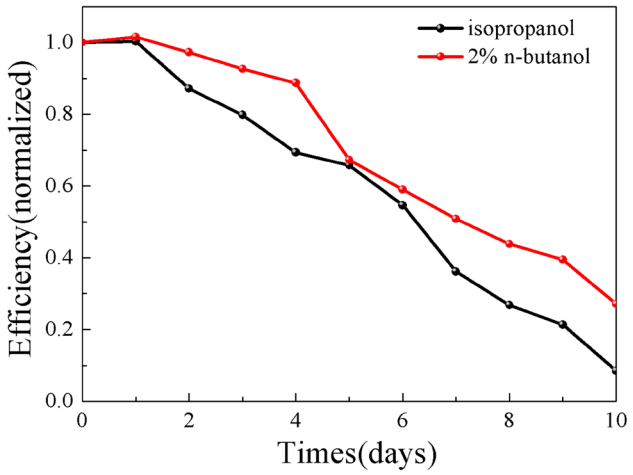

Fig. 5 Device stability of perovskite solar cells fabricated by different solvents

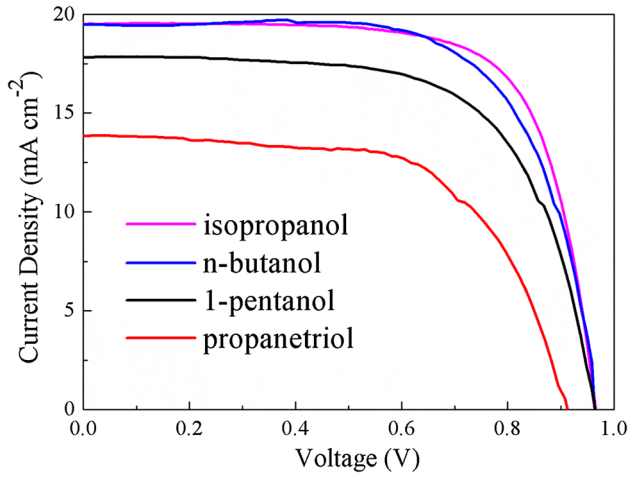

Fig. 6 J–V curves of perovskite solar cells based on different solvents

also investigated another two kinds of solvent, 1-pentanol and propanetriol, which have higher boiling points. The corresponding PSCs presented much lower performance than that of isopropanol, the photovoltaic parameters are listed in Table S1. We think that high boiling point solvent is beneficial to form large perovskite grains, as the slow solvent evaporation, but the low boiling point solvent is useful to form high coverage perovskite film. A balance should be achieved between different solvents.

4 Conclusion

We employed a simple solvent annealing strategy assisted by n-butanol/isopropanol mixed-solvent to improve the quality of perovskite films in two-step deposition method. We found that the perovskite film exhibited larger grain size, higher visible light absorption, and longer carrier lifetime when proper n-butanol was added in isopropanol as solvent for MAI. This improvement could be attributed to the relatively slower solvent evaporation after introduction of n-butanol which is beneficial to perovskite grain growth. Finally, the photovoltaic performance of perovskite solar cells were enhanced from 13.50% to as high as 14.81% when the addition of n-butanol reached to 2% in the mixed-solvents.

Acknowledgements We appreciate the financial supports from Natural Science Foundation of Jiangsu Province (Grant No. BK20160262), the Fundamental Research Funds for the Central Universities (Grant No. 2015XKMS067), and the China Postdoctoral Science Foundation (Grant No. 2016M591952).

References

1. S. Dharani, H.K. Mulmudi, N. Yantara, P.T.T. Trang, N.G. Park, M. Graetzel, S. Mhaisalkar, N. Mathews, P.P. Boix, Nanoscale **6**, 1675 (2014)
2. T. Marimuthu, N. Anandhan, R. Thangamuthu, S. Surya, J. Alloys Compd. **693**, 1011 (2017)
3. L.Z. Liu, Y.Q. Chen, T.B. Guo, Y.Q. Zhu, Y. Su, C. Jia, M.Q. Wei, Y.F. Cheng, ACS Appl. Mater. Interfaces **4**, 17 (2012)
4. T.J. Jacobsson, T. Edvinsson, J. Phys. Chem. C **116**, 15692 (2012)
5. V. Manthina, J.P.C. Baena, G.L. Liu, A.G. Agrios, J. Phys. Chem. C **116**, 23864 (2012)
6. H. Zhang, C. Wang, W.X. Peng, C. Yang, X.H. Zhong, Nano Energy **23**, 60 (2016)
7. H. Sirringhaus, Adv. Mater. **17**, 2411 (2005)
8. J.E. Kroeze, T.J. Savenije, M.J.W. Vermeulen, J.M. Warman, J. Phys. Chem. B. **107**, 7696 (2003)
9. J.J. Shi, Y.H. Luo, H.Y. Wei, J.H. Luo, J. Dong, S.T. Lv, J.Y. Xiao, Y.Z. Xu, L.F. Zhu, X. Xu, ACS Appl. Mater. Interfaces **6**, 9711 (2014)
10. Y. Yang, J. Song, Y.L. Zhao, L. Zhu, X.Q. Gu, Y.Q. Gu, M. Che, Y.H. Qiang, J. Alloys Compd. **684**, 680 (2016)
11. J. Song, Y. Yang, Y.L. Zhao, M. Che, L. Zhu, X.Q. Gu, Y.H. Qiang, Mater. Sci. Eng. B **217**, 18 (2017)
12. J. Wang, L. Zhu, B. Zhao, Y. Zhao, J. Song, X. Gu, Y. Qiang, Sci. Rep. **7**, 14478 (2017)
13. J. Xi, Z. Wu, K. Xi, H. Dong, B. Xia, T. Lei, F. Yuan, W. Wu, B. Jiao, X. Hou, Nano Energy **26**, 438 (2016)
14. B. Xia, Z. Wu, H. Dong, J. Xi, W. Wu, T. Lei, K. Xi, F. Yuan, B. Jiao, L. Xiao, Q. Gong, X. Hou, J. Mater. Chem. A **4**, 6295 (2016)
15. C.F. Lan, J.T. Luo, S. Zhao, C. Zhang, W.G. Liu, S.Z. Hayase, T.L. Ma, J. Alloys Compd. **701**, 834 (2017)
16. Y.T. Shi, Y.J. Xing, Y. Li, Q.S. Dong, K. Wang, Y. Du, X.G. Bai, S.F. Wang, Z.J. Chen, T.L. Ma, J. Phys. Chem. C **119**, 15868 (2015)
17. D. Khatiwada, S. Venkatesan, N. Adhikari, A. Dubey, A. Mitul, L. Mohammad, A. Iefanova, S.B. Darling, Q.Q. Qiao, J. Phys. Chem. C **119**, 25747 (2015)
18. Y.Z. Wu, A. Islam, X.D. Yang, C.J. Qin, J. Liu, K. Zhang, W.Q. Peng, L.Y. Han, Energy Environ. Sci. **7**, 2934 (2014)
19. S. Mabrouk, A. Dubey, W.F. Zhang, N. Adhikari, B. Bahrami, M.N. Hasan, S.F. Yang, Q.Q. Qiao, J. Phys. Chem. C **120**, 24577 (2016)

20. H. Zhang, J. Mao, H.X. He, D. Zhang, H.L. Zhu, F.X. Xie, K.S. Wong, M. Grätzel, W.C.H. Choy, Adv. Eng. Mater. **5**, 1501354 (2015)
21. N. Ahn, D.Y. Son, I.H. Jang, S.M. Kang, M. Choi, N.G. Park, J. Am. Chem. Soc. **137**, 8696 (2015)
22. Z. Xiao, Q. Dong, C. Bi, Y. Shao, Y. Yuan, J. Huang, Adv. Mater. **26**, 6503 (2014)
23. B.G. Zhao, L. Zhu, Y.L. Zhao, Y. Yang, J. Song, X.Q. Gu, Z. Xing, Y.H. Qiang, J. Mater. Sci.: Mater. Electron. **27**, 10869 (2016)
24. S.P. Li, Y.L. Zhao, X.Q. Gu, Y.H. Qiang, N. Tan, J. Mater. Sci.: Mater. Electeon. **28**, 13626 (2017)
25. X. Liu, X.X. Xia, Q.Q. Cai, F.L. Cai, L.Y. Yang, Y. Yan, T. Wang, Sol. Energy Mater. Sol. Cells **159**, 143 (2017)
26. J. Song, S.P. Li, Y.L. Zhao, J. Yuan, Y. Fang, L. Zhu, X.Q. Gu, Y.H. Qiang, J. Alloys Compd. **694**, 1232 (2017)
27. M. Che, L. Zhu, Y.L. Zhao, D.S. Yao, X.Q. Gu, J. Song, Y.H. Qiang, Mater. Sci. Semicond. Process. **56**, 29 (2016)
28. Q. Zhao, G.R. Li, J. Song, Y. Zhao, Y. Qiang, X.P. Gao, Sci. Rep. **6**, 38670 (2016)
29. B.X. Chen, H.S. Rao, W.G. Li, Y.F. Xu, H.Y. Chen, D.B. Kuang, C.Y. Su, J. Mater. Chem. A **4**, 5647 (2016)
30. H.J. Snaith, A. Abate, J.M. Ball, G.E. Eperon, T. Leijtens, N.K. Noel, S.D. Stranks, J.T.W. Wang, K. Wojciechowski, W. Zhang, J. Phys. Chem. Lett. **5**, 1511 (2014)
31. H.-S. Kim, N.-G. Park, J. Phys. Chem. Lett. **5**, 2927 (2014)
32. N. Arora, M.I. Dar, A. Hinderhofer, N. Pellet, F. Schreiber, S.M. Zakeeruddin, M. Grätzel, Science **358**, 768 (2017)